minerals

MDPI

Article

Fe, Mn and ^{238}U Accumulations in *Phragmites australis* Naturally Growing at the Mill Tailings Pond; Iron Plaque Formation Possibly Related to Root-Endophytic Bacteria Producing Siderophores

Yukihiro Nakamoto [1], Kohei Doyama [1], Toshikatsu Haruma [2], Xingyan Lu [1], Kazuya Tanaka [3], Naofumi Kozai [3], Kenjin Fukuyama [4], Shigeru Fukushima [4], Yoshiyuki Ohara [4] and Keiko Yamaji [1,*]

[1] Graduate School of Life and Environmental Sciences, University of Tsukuba, 1-1-1, Tennodai, Tsukuba 305-8587, Japan; s1830272@s.tsukuba.ac.jp (Y.N.); s1930326@s.tsukuba.ac.jp (K.D.); s2030288@s.tsukuba.ac.jp (X.L.)
[2] Division of Sustainable Resources Engineering, Faculty of Engineering, Hokkaido University, Sapporo 060-8628, Japan; haruma.toshikatsu@eng.hokudai.ac.jp
[3] Advanced Science Research Center, Japan Atomic Energy Agency, 2-4, Shirakata, Tokai 319-1195, Japan; tanaka.kazuya@jaea.go.jp (K.T.); kozai.naofumi@jaea.go.jp (N.K.)
[4] Ningyo-toge Environmental Engineering Center, Japan Atomic Energy Agency, 1550, Kamisaibara, Kagamino 708-0698, Japan; fukuyama.kenjin@jaea.go.jp (K.F.); fukushima.shigeru@jaea.go.jp (S.F.); ohara.yoshiyuki@jaea.go.jp (Y.O.)
* Correspondence: yamaji.keiko.fp@u.tsukuba.ac.jp; Tel.: +81-29-853-6850

Abstract: Mine drainage is a vital water problem in the mining industry worldwide because of the heavy metal elements and low pH. Rhizofiltration using wetland plants is an appropriate method to remove heavy metals from the water via accumulation in the rhizosphere. *Phragmites australis* is one of the candidate plants for this method because of metal accumulation, forming iron plaque around the roots. At the study site, which was the mill tailings pond in the Ningyo-toge uranium mine, *P. australis* has been naturally growing since 1998. The results showed that *P. australis* accumulated Fe, Mn, and ^{238}U in the nodal roots without/with iron plaque compared with other plant tissues. Among the 837 bacterial colonies isolated from nodal roots, 88.6% showed siderophore production activities. Considering iron plaque formation around *P. australis* roots, we hypothesized that microbial siderophores might influence iron plaque formation because bacterial siderophores have catechol-like functional groups. The complex of catechol or other phenolics with Fe was precipitated due to the networks between Fe and phenolic derivatives. The experiment using bacterial products of root endophytes, such as *Pseudomonas* spp. and *Rhizobium* spp., showed precipitation with Fe ions, and we confirmed that several *Pseudomonas* spp. and *Rhizobium* spp. produced unidentified phenolic compounds. In conclusion, root-endophytic bacteria such as *Pseudomonas* spp. and *Rhizobium* spp., isolated from metal-accumulating roots of *P. australis*, might influence iron plaque formation as the metal accumulation site. Iron plaque formation is related to tolerance in *P. australis*, and *Pseudomonas* spp. and *Rhizobium* spp. might indirectly contribute to tolerance. Although there are many issues to be resolved in this research, we hope that the fundamental analysis of plant-microbe interactions would be helpful for phytoremediation at mine sites.

Keywords: mill tailings pond; iron; manganese; uranium; *Phragmites australis*; iron plaque

Citation: Nakamoto, Y.; Doyama, K.; Haruma, T.; Lu, X.; Tanaka, K.; Kozai, N.; Fukuyama, K.; Fukushima, S.; Ohara, Y.; Yamaji, K. Fe, Mn and ^{238}U Accumulations in *Phragmites australis* Naturally Growing at the Mill Tailings Pond; Iron Plaque Formation Possibly Related to Root-Endophytic Bacteria Producing Siderophores. *Minerals* **2021**, *11*, 1337. https://doi.org/10.3390/min11121337

Academic Editors: Sumant Avasarala, Tyler L. Spano and Saglara S. Mandzhieva

Received: 1 November 2021
Accepted: 28 November 2021
Published: 29 November 2021

1. Introduction

Mine drainage is a significant water pollution problem in the mining industry worldwide because of the heavy metal elements and low pH. Mine drainage water needs to be treated to decrease the pollution related risks. Several removal methods for heavy metals have been developed using ion-exchange, chemical and microbial precipitation, and neutralization by caustic soda and soda ash. However, the disposal of large amounts of sludge

is costly, and the efficiency of these technologies varies depending on the metals [1–3]. In addition, metals speciation is an important factor because of the toxicity and the uptake in plants [4,5]. In contrast, utilization of plants to treat contaminated water, soil, and sediments through phytoremediation is considered an effective, low-cost, and sustainable remediation method. Wetland plants are often used to remove contaminants, including metals [3,6,7]. Wetland plants used for phytoremediation are known to accumulate metals in their underground parts to maintain wetland formation. "Rhizofiltration," which is an appropriate remediation method for the wetland plants, is used for the removal of heavy metals from the water via their accumulation in the rhizosphere, including inside and outside of the roots [1,7].

Since 1964, Ningyo-toge mine, has been used for developing industrial technologies for the wet uranium refining process from domestic uranium ore to uranium tetrafluoride, which has finished in 1982. Currently, a mill tailings pond is used as temporary storage sites to treat mine water containing iron, manganese, uranium, etc. [8]. Since 1998, at the mill tailings pond in the Ningyo-toge mine, *Phragmites australis* (Cav.) Trin. ex Steud. have been found to grow naturally [9]. *P. australis*, a wetland plant, is distributed globally, especially in Asia and Europe, from cold temperate regions to hot humid tropical wetlands [6,10]. *P. australis* forms vertical and horizontal rhizomes and develops aerenchyma to transport atmospheric oxygen to the roots [11,12]. In addition, *P. australis* has been reported to be used in artificial wetlands to treat metal wastewater because it accumulates heavy metals and radionuclides in roots [6,7,9,13,14]. Generally, plants accumulating high concentrations of metals should have metal-tolerance mechanisms because such high concentrations cause toxicity to plants [15]. For example, Ederli et al. [12] clarified Cd accumulation and tolerance in *P. australis* roots via a water culture experiment; the concentrations of phytochelatins, which are thiol-rich peptides used for metal detoxification, increased in the roots treated with Cd solution compared with control roots. *P. australis* also accumulated Zn and Cd mainly in the roots, and the concentrations were higher in the following order: intercellular spaces, cell walls, vacuoles, and cytoplasm. Most of them were immobilized in the apoplast or sequestered in the vacuolar lumen [16,17]. In addition, binding proteins with Cd and Zn can prevent their free ions in the cytoplasm, which is one of the mechanisms for detoxification in *P. australis* [16,17]. Higuchi et al. [18] reported that *P. australis* accumulates the complex of Cd with an amylopectin-like α-glucan molecule, which is induced in the stems under Cd stress, indicating a Cd detoxification effect. Additionally, on the root surfaces of wet plants, iron plaque, which is composed mainly of iron hydroxide such as ferrihydrite and goethite, was often observed [19,20]; the iron plaque could adsorb metals because of the high affinity of iron hydroxide for metals [21,22]. The formation of iron plaque contributes to heavy metal tolerance in *P. australis* due to the inhibition of Fe and other metals to enter the root cells [13].

Recently, it has been considered that plant-microbe interactions are essential for clarifying environmental stress tolerance in plants. Root-endophytic bacteria have been reported to enhance the physiological heavy-metal tolerance of plants [23]. Microbial siderophores have influenced metal accumulation and metal tolerance in plants because of their chelating characteristics with metals such as Fe, Zn, and Al, for example. Microbes produce siderophores as one of the secondary metabolites (organic chemicals) under low Fe nutrient conditions via the formation of the complex with Fe [24]; siderophores are considered important because they can mobilize insoluble Fe in soil and supply plant roots as a nutrient element. Siderophores have also been reported to chelate with Fe and other metals [24], and additionally, Braud et al. [25] found a profound influence on siderophore production by pseudomonads even under high heavy metals conditions such as Fe, Cr, Hg, and Pb. Therefore, in this study, the aspect of microbial siderophore, its "chelation with metals" under high concentrations of heavy metals, which would be harmful to microbes and plants, were considered. Considering the chelation of microbial siderophores with metals, their important effects on plants growing under heavy metal stress have been reported to enhance (1) metal accumulation and (2) metal detoxification. For example, *Microbacterium saperdae*,

Pseudomonas monteilii, and *Enterobacter cancerogenus*, producing Zn-chelating compounds, enhanced Zn accumulation in a hyperaccumulator plant, *Thlaspi caerulescens* [26]. As another example, Fe-chelating chemicals produced by *Bacillus thuringiensis* enhanced As, Cu, Pb, Ni, and Zn accumulation in *Alnus firma* [27]. In terms of metal tolerance in plants, Zn-chelating chemicals produced by *Pseudomonas putida* and *Rhodopseudomonas* sp. enhanced Zn accumulation and Zn tolerance in a perennial helophyte, *Cicuta virosa* [28]. Iron plaque is mainly composed of ferrihydrite [20] and in natural-organic matter rich environments, a catechol type compound, 3,4-dihydroxybenzoic acid could chelate Fe (III) and eventually enhanced the organic formation of ferrihydrite [29]. Generally, bacterial siderophores are known to have catechol-like functional groups [30], and Bijlsma et al. [31] reported that the complex of catechol with Fe was precipitated because of the networks between Fe and phenolic derivatives. These networks are called metal-phenol networks (MPNs), and MPNs have appeared as multipurpose surface modifiers based on the universal adherence properties of phenol molecules, including their constituent galol and catechol groups [32].

Given the background described so far, the purpose of this study was to clarify the accumulation of heavy metals in *P. australis* growing at the mill tailings pond in the Ningyo-toge mine, considering the influence of root-endophytic bacteria. The study analyzed (1) metal accumulation in *P. australis* during the growing season and observed (2) Fe localization in nodal roots because Fe was highly contained. Additionally, the study analyzed (3) siderophore production by root-endophytic bacteria isolated from *P. australis* roots, confirmed (4) precipitation by bacterial products with Fe ions, and detected (5) phenolics in the bacterial products. Finally, Fe, Mn and ^{238}U accumulation in *P. australis* via the functional effects of root-endophytic bacteria, considering these metal tolerance in this plant was discussed.

2. Materials and Methods

2.1. Study Site and Collection of P. australis

The mill tailings pond (35°18′46.8″ N, 133°56′19.0″ E) as the study site is located at the Ningyo-toge Environmental Engineering Center, Japan Atomic Energy Agency. Naturally growing *P. australis* was collected in July 2017, September 2017, July 2018, and September 2018. *P. australis* growing straight in the water was collected by cutting the stems under the nodal roots. For each collection time, five individuals, which were at the same growth stage, were collected. An iron plaque has been observed around the roots of *P. australis* growing at the mill tailings pond in the Ningyo-toge mine; nodal roots with/without iron plaque of *P. australis* were collected separately in 2018, in particular.

The Ningyo-Toge Environmental Engineering Center has continuously evaluated water quality data at the mill tailings pond; therefore, the data of elemental concentrations (Fe, Mn, and ^{238}U), temperature, pH, and oxidation-reduction potential (ORP) in 2017 and 2018 at the *P. australis* growing site (water depth: 50 cm) were summarized in Tables 1 and 2. As shown in Table 1, the water contained Fe, Mn, and ^{238}U in both years. As shown in Table 2, the water had a low positive ORP value, indicating a neutral pH.

Table 1. Concentrations of Elements in the Water at *P. australis* Growing Site (Water Depth; 50 cm).

Year	Concentration of Elements		
	Fe (mg/L)	Mn (mg/L)	^{238}U (μg/L)
2017 *	8.54 ± 4.42	0.55 ± 0.21	45.8 ± 26.1
2018 **	15.2 ± 0.80	1.21 ± 0.21	14.9 ± 2.72

Fe and Mn were measured by ICP-OES (Thermo Fisher Scientific iCAP 6300 Duo) and ^{238}U were measured by ICP-MS (Agilent Technologies 7800). * The results in May, August, and December 2017 are expressed as mean ± SE (n = 3). ** The results on May, August, and November in 2018 are expressed as mean ± SE (n = 3).

Table 2. Temperature, pH, and ORP of the Water at *P. australis* Growing Site (Water Depth; 50 cm).

Year	Water Temperature (°C)	pH	ORP (mV)
2017 *	15.8 ± 3.66	6.69 ± 0.18	26.3 ± 35.1
2018 **	16.4 ± 3.27	6.79 ± 0.07	12.0 ± 68.1

The water temperature was measured using a portable electrical conductivity meter (DKK-TOA Corporation CM-31P). The pH and ORP were measured using a portable pH/ORP meter (Kasahara Chemical Instruments Corporation KP-10Z). * The results in May, August, and December 2017 are expressed as mean ± SE (n = 3). ** The results in May, August, and November in 2018 are expressed as mean ± SE (n = 3).

2.2. Analysis of Element Concentrations in Plants, and Calculations of Translocation Factor and Bioconcentration Factor

The plants were carefully washed with tap water and then with deionized water prepared by a Millipore filtration system (Merck, Darmstadt, Germany). *P. australis* was divided into four parts: nodal roots, stems, leaves, and spikes found in September. In 2018, the nodal roots were carefully separated into two types: nodal roots with or without iron plaque. The cleaned plant tissues were dried at 80 °C for 48 h, and each plant tissue was ground. To quantify Fe and Mn in the plant tissues, the ground plant materials were weighed and pyrolyzed using concentrated HNO_3 at 130 °C and analyzed by inductively coupled plasma optical emission spectroscopy (ICP-OES; 720ICP-OES, Agilent Technologies, Santa Clara, CA, USA). The results of the five replications were averaged, and the standard errors (SEs) were calculated.

For the quantification of ^{238}U in plant tissues, according to [33], the ground plant materials were reduced to ashes at 500 °C for 4 h in a box furnace (Koyo, Japan). The ash was weighed and decomposed in concentrated HNO_3. The decomposed sample solution was measured by inductively coupled plasma mass spectrometry (ICP-MS; Agilent7500series, Agilent, Santa Clara, CA, USA). For the nodal roots with iron plaque collected from *P. australis*, decomposition was performed as described above after ashing. Fe and Mn were measured with ICP-OES, and ^{238}U was measured with ICP-MS, and the results of the five replications were averaged, and standard errors (SEs) were calculated.

Translocation factors (TFs) and bioconcentration factors (BCFs) [34,35] using element concentrations of leaves, stems, and nodal roots and the water in each year were calculated. The results of the five replications were averaged, and the standard errors (SEs) were calculated.

2.3. Observation of Iron Localization in P. australis Nodal Roots

According to the elemental analyses of the plant tissues, *P. australis* showed a high accumulation of Fe in the nodal roots; therefore, Fe localization in the nodal roots were observed. Nodal roots with and without iron plaque collected in July and September 2018, were washed as described in 2.2, fixed in glutaraldehyde-phosphoric acid solution after degassing in vacuo for 15 min, and stored at 4 °C before use. Fixed nodal roots were washed twice with deionized water under shaking for 10 min, embedded in 4% agar in the freezer at −80 °C for 30 min, and cut into 100-µm sections with a microtome (REM-710, Yamato Kohki, Saitama, Japan). In this experiment, Fe accumulation in the nodal roots was confirmed by the staining method [36]; the root sections were placed in 2% potassium ferrocyanide (*w*/*v*, 2% HCl) for 15 min in vacuo, kept for 15 min at room temperature, and washed with Millipore water with shaking for 15 min three times. The stained root sections were observed under an optical microscope (CX21, Olympus, Tokyo, Japan); the stained blue sections indicate Fe accumulation.

2.4. Isolation of Endophytic Bacteria from P. australis Nodal Roots, Evaluation of Siderophore-Production Activity by CAS-Fe Assay and Identification

2.4.1. Isolation of Endophytic Bacteria

Nodal roots collected from five individuals of *P. australis* in September 2017 were used to isolate endophytic bacteria. Before isolation, parts of the washed nodal roots, as shown in Section 2.2, were stained with trypan blue to confirm filamentous fungal infections, such as

arbuscular fungi and root-endophytic fungi. According to [37,38], the fungal infection rate of fungi was calculated to be 0.00 ± 0.00% (150 observation points per individual, n = 5); therefore, we focused on bacteria. Washed nodal roots were sterilized with 70% EtOH for 1 min, followed by 15% H_2O_2 for 5 min, and 70% EtOH for 1 min. After sterilization, the nodal roots were washed twice with sterilized water for 5 min. Under the clean bench, sterilized nodal roots were cut into approximately 10 mm, and 200 root sections were prepared per individual. One hundred root sections were incubated on 1% nutrient broth agar (1% NBA), and the other 100 sections were incubated on 1% tryptic soy agar (1% TSA) for 1 month at 23 °C in the dark. Bacterial colonies were isolated three times on 1% TSA or 1% NBA, and 837 colonies were isolated.

2.4.2. Evaluation of Siderophore-Production Activity of Endophytic Bacteria on CAS-Fe Medium and Identification

Isolated 837 bacterial colonies, shown in Section 2.4.1, were used for the assay. Bacterial disks (4.0 mm i.d.) grown on each medium for about 1 week were placed on CAS-Fe medium [39] and incubated at 23°C in the dark for 3 days. The number of bacterial colonies was too high, and therefore, one replication was set for each colony. After 3 days, the diameters of clear zones and colonies were vertically measured at two points per colony, and the average was used for the calculation of siderophore production activity using the following formula:

$$\text{Siderophore production acitvity} = \frac{\text{Clear zone diameter} - \text{Colony diameter}}{\text{Colony diameter}} \quad (1)$$

When the bacterial colonies showed a slightly clear zone, the diameters of which could not be measured, we evaluated them as having low production of siderophores.

For the top-10 bacteria showing production activities, their activities were examined again on CAS-Fe medium as described above in three replications. These bacteria were identified using DNA analyses. According to the manufacturer's protocol, bacterial DNA was extracted from a single colony isolated on a plate using PrepMan Ultra Reagent (Applied Biosystems, Waltham, MA, USA). The bacterial 16S rRNA gene was amplified using the primer pairs 27F (5′-AGA GTT TGA TCC TGG CTC AG-3′) and 1492R (5′-GGT TAC CTT GTT ACG ACT T-3′) [40] with Ex Taq DNA polymerase (TaKaRa Bio Inc., Shiga, Japan) [41]. After purification, the PCR products were sequenced using a 3730XL DNA Analyzer (Applied Biosystems) with a BigDye Terminator version 3.1 Cycle Sequencing Kit (Applied Biosystems) using 341F (50-CCTACGGGAGGCAGC AG-30) [42] as a sequencing primer. A homology search was done via the BLAST program provided by the DNA Data Bank of Japan (http://blast.ddbj.nig.ac.jp/ (accessed on 17 January 2018)).

2.5. Confirmation of Precipitation by Bacterial Culture Filtrate with Fe Ions and Phenolic Production by HPLC

Root-endophytic bacteria (10 isolates), which showed high siderophore production activities, as shown in Section 2.4.1, were used. Each bacterial disk (8 mm) grown on 1% TSA or 1% NBA for 3 days at 23 °C was inoculated into the rhizosphere medium (RSM; 30 mL in 50 mL flask) [43] under shaking conditions (150 rpm) for 60 h at 23 °C. After incubation, the bacterial medium was filtered through a sterilized 0.20 µm-cellulose acetate filter (Advantec, Tokyo, Japan). The filtrate was evaporated in vacuo at 40–45 °C and 4-times concentrated bacterial filtrate was used to confirm (1) precipitation by bacterial culture filtrate with Fe ions and (2) phenolic production by HPLC. Before the experiments, the siderophore production activity of bacterial filtrates was confirmed on CAS-Fe medium as follows. A sterilized stainless cup (8 mm i.d.) with an open bottom was placed on CAS-Fe medium and 4-times concentrated bacterial filtrate (200 µL) was placed into a cup. After 36-h incubation at 23 °C, siderophore production activity was evaluated by measuring the diameters of clear zones vertically measured at two points per cup. The results of three replications were averaged, and standard errors (SEs) were calculated.

For the first experiment, the precipitation was confirmed by mixing 4-times concentrated bacterial filtrates with Fe^{2+} or Fe^{3+} as follows; 4-times concentrated bacterial filtrates (500 µL) were mixed with 2 mM $FeSO_4$ (Fe^{2+}, 500 µL) or 2 mM $FeCl_3$ (Fe^{3+}, 500 µL) in 40 mM MES (pH 5.5). After 3 h, precipitation was observed compared with the control solution, a mixture of 4-times concentrated RSM (500 µL) with 2 mM $FeSO_4$ (Fe^{2+}, 500 µL) or 2 mM $FeCl_3$ (Fe^{3+}, 500 µL) in 40 mM MES (pH 5.5). We also set up other controls; 4-times concentrated bacterial filtrates (500 µL) mixed with 40 mM MES (pH 5.5, 500 µL) without Fe ions. Bacterial siderophores are known to have catechol-like functional groups [30]; therefore, we also confirmed the precipitation in a mixture of catechol (Wako, Japan) with Fe^{2+} or Fe^{3+} as follows: catechol solution (0, 0.125, 0.25, 0.5, 1, or 2 mM in water, 1 mL) was mixed with 2 mM $FeSO_4$ (Fe^{2+}, 1 mL) or 2 mM $FeCl_3$ (Fe^{3+}, 1 mL) in 40 mM MES (pH 5.5). For the control, each catechol solution (1 mL) was mixed with 40 mM MES (pH 5.5, 1 mL) without Fe. Three replicates were prepared for each treatment. Precipitation was also observed using an optical microscope (CX21, Olympus, Tokyo, Japan).

For the second experiment, phenolics in the bacterial culture filtrates were analyzed by high-performance liquid chromatography (HPLC; Prominence UFLC series, Shimadzu, Japan) with a diode array detector (DAD; SPD-M20A, Shimadzu, Japan) due to the analytical condition using gradient solvent system; (A) methanol, and (B) 1.5% tetrahydrofuran and 0.25% phosphoric acid in Millipore water due to [44]. For the HPLC column, Mightysil RP-18GP, 75 mm × 4.6 mm i.d. (Kanto Chemical Co., Inc., Tokyo, Japan) was used. 4-times concentrated bacterial filtrate (10 µL) was injected into HPLC-DAD, and the UV spectrum between 220 and 400 nm of each peak was confirmed. To qualify the bacterial filtrates, the spectral characteristics were carefully checked and compared with general phenolics, such as catechol, coniferyl alcohol, chlorogenic acid, resorcinol, protocatechuic acid, cinnamic acid, gallic acid, catechins, flavonoids, ellagic acid, and so on. These UV spectra data have been stored in the library of the HPLC system, made by analyzing purchased standard chemicals.

2.6. Statistical Analysis

The results were analyzed using SPSS Statistics software (ver. 25.0, IBM, Armonk, NY, USA). The differences in the concentrations of each element (Fe, Mn, or ^{238}U) between plant tissues at each sampling time were evaluated by a one-factorial analysis of variance (one-factorial ANOVA) with Scheffé post hoc test. The differences in TFs and BCFs between plant tissues at each sampling time were evaluated by Student's *t*-test and one-way ANOVA with Scheffé post hoc test. Differences were considered significant at $p < 0.05$.

3. Results

3.1. Elemental Concentrations of P. australis

Fe and Mn were detected in all plant tissues (Figure 1A,B), and Fe concentrations were significantly higher in the nodal roots (Figure 1A). Mn concentrations were significantly higher in nodal roots than in stems and spikes (Figure 1B). ^{238}U was mainly detected in nodal roots (Figure 1C). In the nodal roots with iron plaque, Fe, Mn, and ^{238}U were also detected (Figure 2). Other metals, such as Cd, Cu, Ni, and Pb, were not detected in the plants.

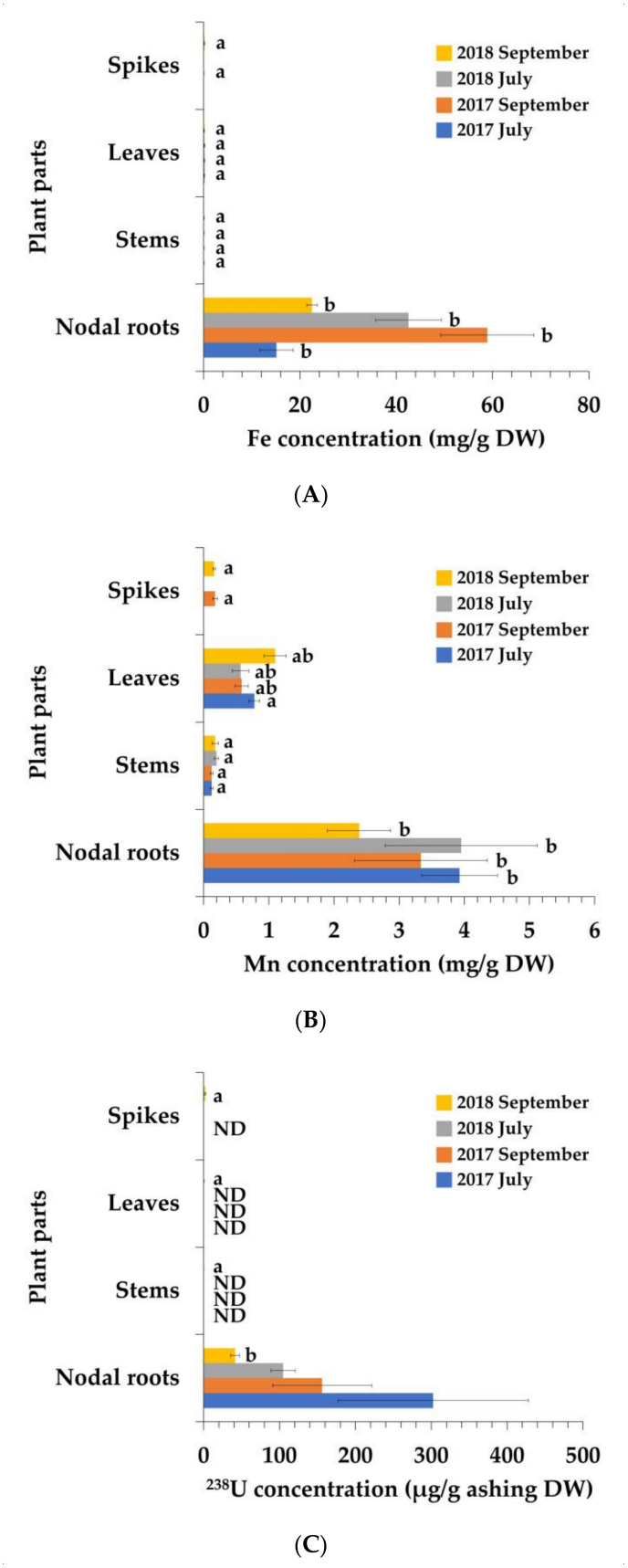

Figure 1. Concentrations of elements in *P. australis*; (**A**) Fe concentrations in the tissues; (**B**) Mn concentrations in the tissues; (**C**) ^{238}U concentrations in the tissues. ND indicates under the detection limit. The results expressed as means ± SEs (n = 5).

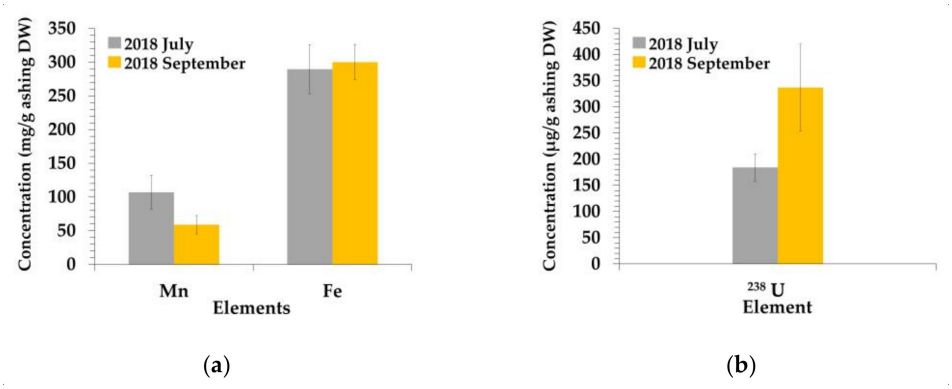

Figure 2. Concentrations of elements in nodal roots with iron plaque *P. australis* in 2018; (**a**) Fe and Mn concentrations; (**b**) ^{238}U concentrations. The results expressed as means ± SEs (n = 5).

3.2. Translocation Factors (TFs) and Bioconcentration Factors (BCFs)

The results of the metals TFs and BCFs are listed in Tables 3 and 4, respectively. All metal TFs (Table 3) were lower than the 1. Fe's leaves/nodal roots TFs were significantly higher than stems/nodal roots TFs in September 2017 and September 2018. With respect to Mn, leaves/nodal roots TFs were significantly higher than stems/nodal roots TFs, except in July 2018. For ^{238} U, stems/nodal roots TF was significantly higher than leaves/nodal roots TF in September 2018. In addition, Fe BCFs of the nodal roots were significantly higher than those the BCFs of stems and leaves at all collection times (Table 4). Mn BCFs of nodal roots were significantly higher than the BCFs of stems and leaves in July 2017. ^{238} U BCF of nodal roots was significantly higher than the BCF of leaves and stems in September 2018.

Table 3. Translocation Factors (TFs) of Elements in *P. Australis* Collected in 2017 and 2018.

Elements	July, 2017		September, 2017	
	Stems/Nodal Roots	Leaves/Nodal Roots	Stems/Nodal Roots	Leaves/Nodal Roots
Fe	$0.05 \times 10^{-1} \pm 0.01 \times 10^{-1}$	0.01 ± 0.00	$0.01 \times 10^{-1} \pm 0.01 \times 10^{-1}$	$0.03 \times 10^{-1} \pm 0.01 \times 10^{-1}$ **
Mn	0.03 ± 0.00	0.21 ± 0.03 **	0.05 ± 0.01	0.22 ± 0.06 *
^{238}U	—	—	—	—
Elements	**July, 2018**		**September, 2018**	
	Stems/Nodal Roots	**Leaves/Nodal Roots**	**Stems/Nodal Roots**	**Leaves/Nodal Roots**
Fe	$0.02 \times 10^{-1} \pm 0.01 \times 10^{-1}$	$0.04 \times 10^{-1} \pm 0.01 \times 10^{-1}$	$0.04 \times 10^{-1} \pm 0.01 \times 10^{-1}$	$0.07 \times 10^{-1} \pm 0.01 \times 10^{-1}$ *
Mn	0.06 ± 0.01	0.19 ± 0.05	0.08 ± 0.03	0.53 ± 0.10 *
^{238}U	—	—	$0.04 \times 10^{-1} \pm 0.01 \times 10^{-1}$ *	$0.01 \times 10^{-1} \pm 0.02 \times 10^{-1}$

The results are expressed as the mean ± SE (n = 5). — indicates that the values could not be calculated because the element concentrations in the stems and leaves were below the detection limit. Student's *t*-test; * $p < 0.05$, ** $p < 0.01$.

Table 4. Bioconcentration Factors (BCFs) of Elements in *P. australis* Collected in 2017 and 2018.

Elements	July, 2017			September, 2017		
	Nodal Roots	Stems	Leaves	Nodal Roots	Stems	Leaves
Fe	1770 ± 409 a	7.28 ± 0.23 b	19.7 ± 1.54 b	6900 ± 1130 a	7.64 ± 0.81 b	21.1 ± 2.56 b
Mn	7140 ± 1060 a	224 ± 36.2 b	1420 ± 152 b	6060 ± 1860 a	222 ± 40.5 b	1060 ± 179 ab
^{238}U	6610 ± 2740	—	—	3410 ± 1430	—	—
Elements	**July, 2018**			**September, 2018**		
	Nodal Roots	**Stems**	**Leaves**	**Nodal Roots**	**Stems**	**Leaves**
Fe	2800 ± 448 a	4.61 ± 0.53 b	10.7 ± 3.43 b	1480 ± 71.7 a	6.09 ± 1.18 b	9.70 ± 0.49 b
Mn	3270 ± 967 a	163 ± 27.0 b	468 ± 105 ab	1970 ± 401 a	146 ± 40.1 b	906 ± 140 ab
^{238}U	7030 ± 1070	—	—	2780 ± 411 a	10.4 ± 2.16 b	30.1 ± 6.84 b

The results are expressed as the mean ± SE (n = 5). — indicates that the values could not be calculated owing to the data (leaves and stems) below the detection limit. Different letters indicate significant differences between plant tissues at each sampling time evaluated by one-factorial ANOVA with Scheffé post hoc test ($p < 0.05$).

3.3. Fe Localization in the Nodal Roots of P. australis

The results are shown in Figure 3. Fe localization was observed only in the epidermal cells of the nodal roots without iron plaque (Figure 3b). In contrast, Fe localization was observed within the iron plaque in the nodal roots with iron plaque (Figure 3d).

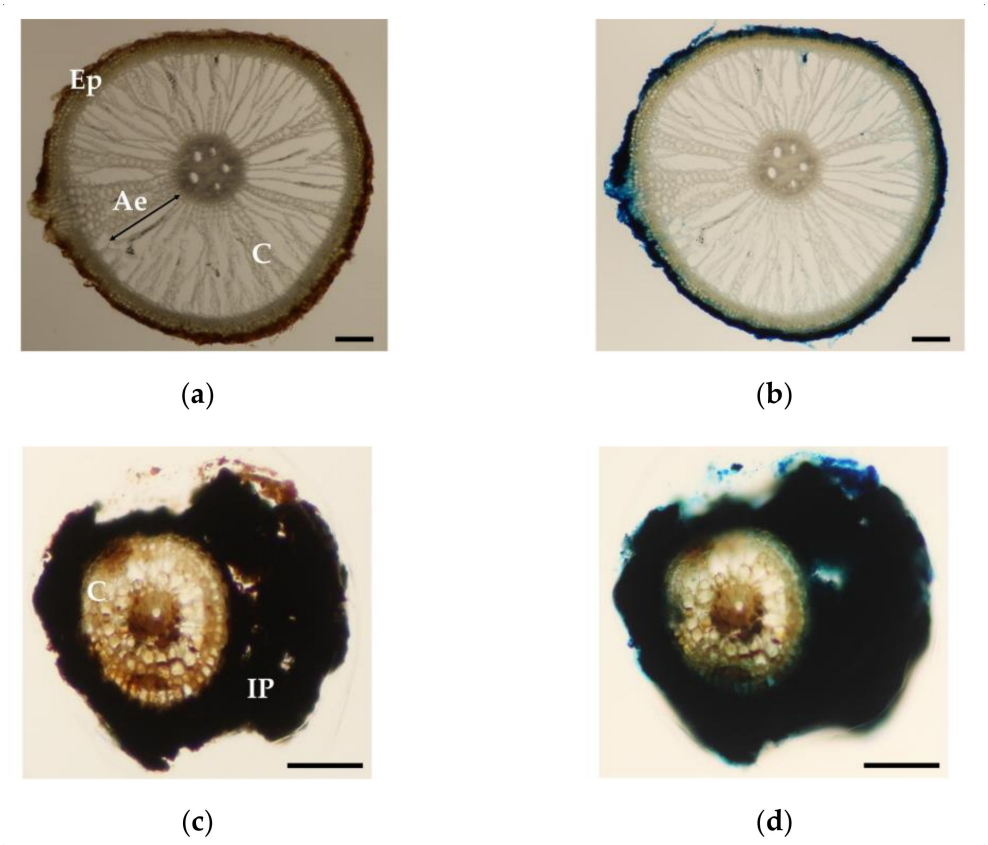

Figure 3. Fe localization in nodal root sections of *P. australis*. (**a**,**b**) Nodal roots without iron plaque. (**c**,**d**) Nodal roots with iron plaque. All photos were taken under the optical microscope. Left photos shown in (**a**,**c**), were the roots before staining and right photos shown in (**b**,**d**) were the roots after staining; blue area indicates Fe localization. Ep: epidermis. C: cortex. Ae: aerenchyma. IP: iron plaque. Scale bars represent 100 μm.

3.4. Siderophore Production Activity by Root-Endophytic Bacteria Isolated from P. australis

A total of 417 and 420 bacterial colonies were isolated on 1% NBA and 1% TSA, respectively. Among the 837 bacterial colonies in total, 742 colonies (382 colonies isolated on 1% NBA and 360 colonies isolated on 1% TSA) corresponding to 88.6% showed siderophore production activities. A total of 233 colonies (121 colonies isolated on 1% NBA and 112 colonies isolated on 1% TSA) showed low production of siderophores, which means that clear zones were too small to measure. 33 colonies (16 colonies isolated on 1% NBA and 17 colonies isolated on 1% TSA) could not grow on CAS-Fe medium. 62 colonies (19 colonies isolated on 1% NBA and 43 colonies isolated on 1% TSA) did not show any activity. A total of 509 bacterial colonies, corresponding to 60.8%, clearly showed siderophore production activities (Figure 4). Based on the DNA analysis of bacterial isolates, the top-10 bacteria showing high siderophore production activities were identified as *Pseudomonas* spp., *Herbaspirillum* spp., and *Rhizobium* spp. (Table 5).

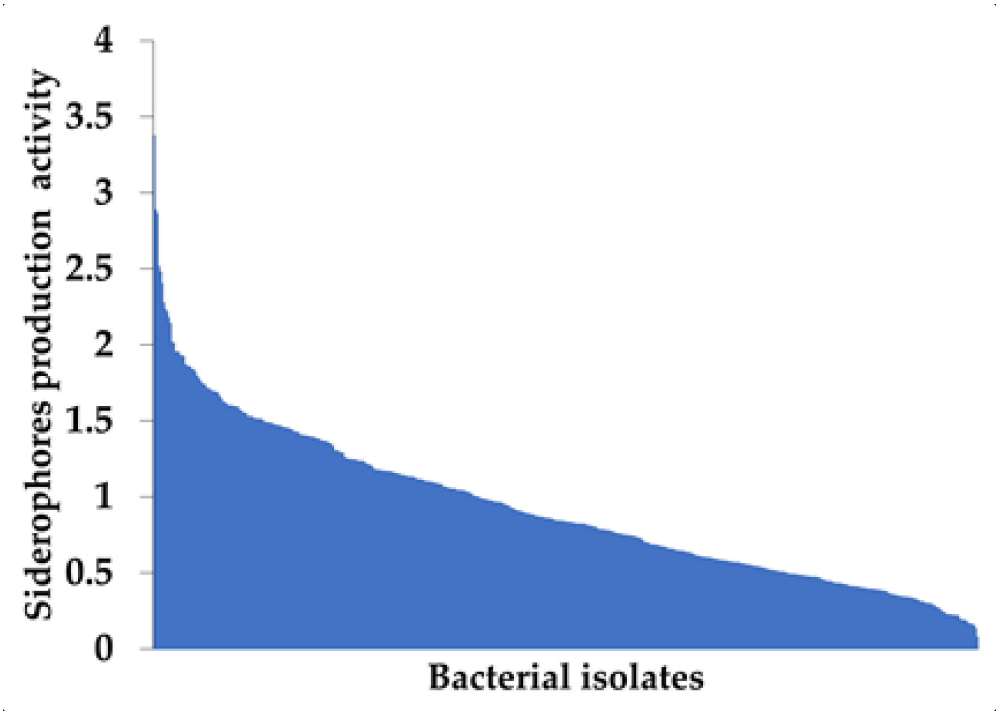

Figure 4. Siderophore production activities of root-endophytic bacteria isolated from *P. australis*. 509 colonies were sorted from left to right in order of highest activity. Additionally, 233 colonies showed low production of siderophore.

Table 5. Endophytic Bacteria Species Showing High Siderophore Production Activity.

Bacterial Isolates	Siderophore Production Activity *	Species Name
T1-66	3.16 ± 0.01	*Pseudomonas rhodesiae* strain VTT E-031889
T5-48	3.15 ± 0.03	*Herbaspirillum* sp. ZX2
T1-42	3.12 ± 0.04	*Pseudomonas putida* strain S975
N5-48	3.10 ± 0.05	*Pseudomonas rhodesiae* strain VTT E-031889
T4-20	3.04 ± 0.02	*Pseudomonas rhodesiae* strain VTT E-031889
N4-46	2.87 ± 0.04	*Rhizobium nepotum*
N2-80	2.83 ± 0.05	*Herbaspirillum* sp. AU2339
T1-11	2.71 ± 0.09	*Pseudomonas extremaustralis* strain OX0322
T4-45	2.33 ± 0.27	*Herbaspirillum* sp. Os43
N1-76	2.17 ± 0.16	*Pseudomonas protegens* strain FDAARGOS_307

* The results are expressed as the mean ± SE (n = 3).

3.5. Confirmation of Precipitation by Bacterial Culture Filtrate with Fe Ions and Phenolic Production by HPLC

Catechol, a functional group of bacterial siderophores [30], was used for the test; precipitation with Fe ions was observed (Figure 5a). For the bacterial culture filtrate with Fe ions, differences between the isolates were observed; in the culture filtrates of T1-66, T1-42, N5-48, T4-20 (Figure 5b), N4-46, T1-11, and N1-76 (Figure 5c), the precipitation with Fe ions were found. *Herbaspirillum* spp., such as T5-48, N2-80, and T4-45, did not show precipitation (Figure 5b,c). In particular, in N4-46, N5-48, and T1-11 culture filtrates with Fe ions, compared with the control, different precipitation was observed under the microscope; the size of the precipitation observed in the culture filtrates was larger than that in RSM. Additionally, significant precipitation was observed in the N4-46 culture filtrate.

HPLC-DAD analysis results showed that two phenolic peaks (retention time, approximately 23.2 min and 26.2 min) were found in the T1-66, N5-48, T4-20 bacterial culture filtrates N4-46, and N1-76 compared with RSM as a control (Figure 6a). Compared with RSM, peaks at around 1.0–1.3 min were found in the culture filtrates; these peaks were

considered to be related to organic acids. UV spectra (220–400 nm) of peaks at 23.2 min and 26.2 min in T1-66 culture filtrate were shown in Figure 6B. UV spectra of peaks at 23.2 min and 26.2 min showed maximum absorbance at around 260 nm, related to benzene ring, and similar characteristics to those of phenolics. The absorbance between 260 and 400 nm indicates that phenolic hydroxyl groups influence shifts to longer wavelengths; however, the UV spectra were not matched to those of general phenolics, including catechol in the library data. The identical spectra of the peaks at the exact retention times were also confirmed in the N5-48, T4-20, N4-46, and N1-76 culture filtrates. Table 6 summarizes all the results of the precipitation and HPLC results described above.

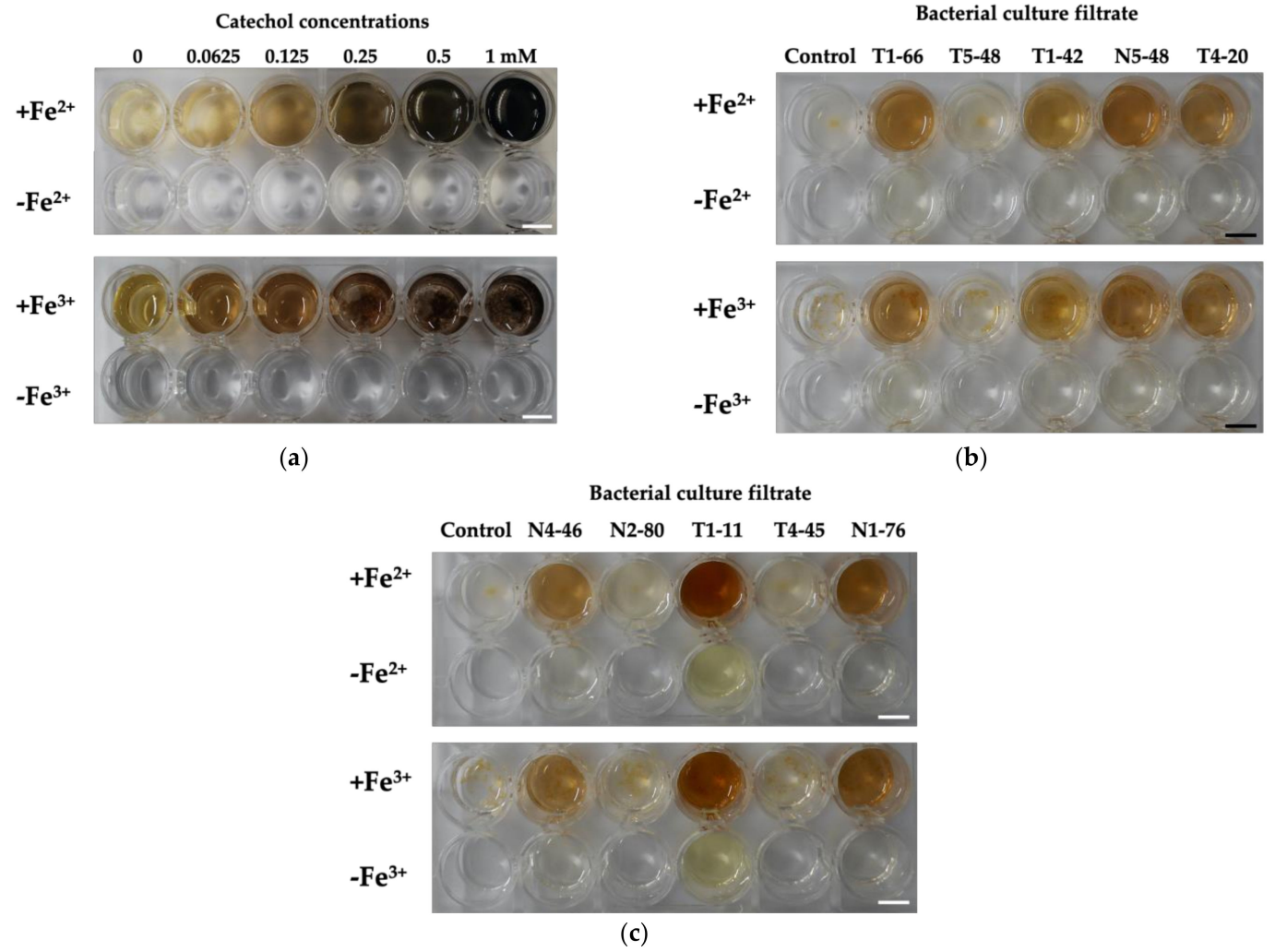

Figure 5. Precipitation in the mixture of bacterial culture filtrates or catechol solution with Fe ions. (**a**) Confirmation of the precipitation of catechol with Fe ions. (**b**,**c**) Precipitation in the mixture of bacterial culture filtrates and Fe ions. (**a**–**c**); scale bars represent 5 mm.

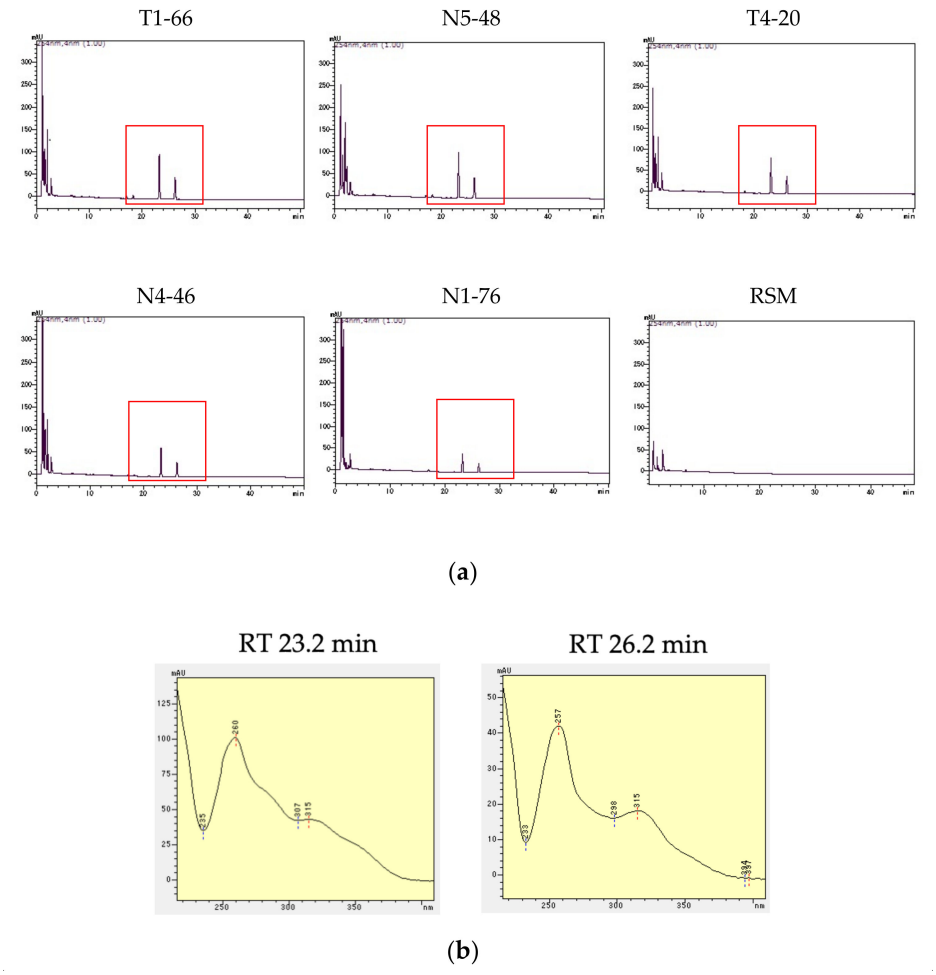

Figure 6. Phenolics in bacterial culture filtrates. (**a**) HPLC chromatogram of bacterial culture filtrates of the isolates, in which phenolic peaks were found at 254 nm. At retention time (RT), around 23.2 min and 26.2 min, peaks were confirmed in the bacterial filtrates. In HPLC chromatogram of RSM medium as a control, these peaks were not found. (**b**) Spectra between 220 nm and 400 nm of two peaks found in T1-66 culture filtrate at 23.23 min and 26.21 min, respectively. Same spectrum at each RT was also confirmed in each peak detected in N5-48, T4-20, N4-46, and N1-76 culture filtrates.

Table 6. Bacterial Culture Filtrate Characteristics on Siderophore Production Activity, precipitation with Fe ions and phenolic production.

Isolates	Siderophore Production Activity * (Clear-Zone Diameter, mm)	Precipitation with Fe Ions **	Phenolic Production ***
T1-66	37.7 ± 0.07	+	+
T5-48	26.4 ± 1.10	–	–
T1-42	25.3 ± 0.61	+	–
N5-48	35.6 ± 0.34	+	+
T4-20	33.4 ± 0.59	+	+
N4-46	32.6 ± 0.15	+	+
N2-80	27.3 ± 0.43	–	–
T1-11	38.1 ± 0.13	+	–
T4-45	25.6 ± 0.20	–	–
N1-76	32.1 ± 0.66	+	+

* The results of siderophore production activities on CAS-Fe medium are expressed as mean ± SE (n = 3). ** + indicates the confirmation of the precipitation with Fe^{2+} and Fe^{3+} ions and—indicates no precipitation with Fe ions in three replications. *** + indicates phenolic products detection and—indicates no detection of phenolics by HPLC-DAD.

4. Discussion

Phragmites australis growing naturally at the mill tailings pond in Ningyo-toge mine significantly accumulated Fe and Mn in the nodal roots (Figure 1A,B) compared with the concentrations generally found in plants (Fe, 0.018–1.51 mg/g DW; Mn, 0.016–1.84 mg/g DW) [45]. TF and BCF values also indicate that *P. australis* accumulated these metals in the nodal roots compared with the leaves and stems (Tables 1 and 2). These results seem similar to those of *P. australis*, as shown in [14,46]. ^{238}U was significantly accumulated in the nodal roots compared with stems, leaves, and spikes (Figure 1C), and the concentrations in the nodal roots were approximately 40–300 μg/g ashing DW. [14] similarly reported that ^{238}U concentration in *P. australis* roots (82.8 ± 24.0 μg/g) and the concentration in the aboveground part was low compared with the roots. [47] clarified at Sevilha mine that ^{238}U concentrations of wetland plants such as *Callitriche stagnalis*, *Lemna minor*, and *Riccia fluitans* were 55.6 μg/g DW, 53.0 μg/g DW and 50.6 μg/g DW, respectively. In comparison with these results, the nodal roots with/without iron plaque of *P. australis* observed in this study showed higher ^{238}U accumulation. In the nodal roots with iron plaque, Fe, Mn, and ^{238}U also got accumulated (Figure 2). However, these concentrations cannot be directly compared with the ones shown in Figure 1 because the decomposition procedures differed. Furthermore, Fe localization was found in epidermal root cells and in iron plaque around the nodal roots, but not in the cortical cells (Figure 3), indicating that the main Fe accumulation sites in *P. australis* were epidermal root cells and iron plaque outside of the roots. This Fe accumulation in iron plaque might enhance heavy metal tolerance in the roots, because an iron plaque acts as a barrier against Zn in a wetland plant, *Aster tripolium* [48]. Iron plaque formation around the roots seems to be important for the accumulation site, and this formation might enhance heavy metal tolerance in the roots.

Due to the bacterial isolation from *P. australis* nodal roots, many root-endophytic bacteria showed high siderophore production activities on CAS-Fe medium (Figure 4). Among them, the top-10 bacteria showing siderophore production activities were *Pseudomonas* spp., *Herbaspirillum* spp., and *Rhizobium* spp. (Table 5). Generally, many bacterial siderophores have catechol-like functional groups [30], and a complex of catechol with Fe and precipitation has been reported [31]. In addition, the complex of tannic acid and pyrogallol with Fe is also known to precipitate [49,50]. In iron plaque, ferrihydrite was mainly confirmed [20] and, for ferrihydrite found in the natural-organic matter rich environments, hydroxybenzoic acid moieties effectively suppressed the inorganic formation of ferrihydrite, because hydroxybenzoic acid could chelate Fe (III) species at double corner-sharing Fe-Fe linkages [29]. Furthermore, natural organic matter could enhance the organic formation of ferrihydrite, compared with inorganic ferrihydrite [29]. Therefore, we hypothesized that microbial siderophores might influence iron plaque formation. In the experiment, the precipitation of catechol and Fe ions was firstly confirmed (Figure 5a). In the results, in the mixture of bacterial culture filtrate of T1-66, T1-42, N5-48, T4-20, N4-46, T1-11, or N1-76 with Fe ions, precipitation was observed (Figure 5b,c). Based on HPLC-DAD analysis using bacterial culture filtrates, two phenolics showing the same retention time and UV spectra were found in the bacterial culture filtrates of T1-66, N5-48, T4-20, N4-46, and N1-76, but not in RSM (Figure 6a and Table 6), indicating that these phenolics might influence iron plaque formation via precipitation with Fe ions. In contrast, in bacterial filtrates of T1-42 and T1-11, which showed precipitation with Fe ions (Figure 5b,c), peaks related to phenolics were not found by HPLC-DAD. In these filtrates, polar chemical compounds, such as organic acids, were detected at an early retention time (data not shown). Microbial siderophores have diverse chemical structures [51]. *Pseudomonas* species are known to produce various kinds of siderophores, such as pyoverdins [52], pyoverdine B10 [53], pyochelin [54], quinolobactin [55], corrugatin [56], ornicorrugatin [57], and pseudomonine [58]. *Herbaspirillum* species are known to produce serobactins [59], and *Rhizobium* are known to produce rhizobactin [60], vicibactin [61], schizokinen [62], 2,3-dihydroxy benzoic acid [63] and unidentified catechol-type siderophore [64]. Among them, pyoverdins, pyoverdine B10, pyochelin, pseudomonine, and 2,3-dihydroxy benzoic acid are phenolic

compounds. Therefore, other possible phenolic chemicals may influence the formation of iron plaques. These results suggest the possible influence of bacterial siderophores on iron plaque formation; if the influence of bacterial products on iron plaque formation is clarified, we need to purify bacterial siderophores to be identified via instrumental analyses, such as NMRs and MSs, and to confirm the precipitation with Fe ions using purified bacterial siderophores. Furthermore, to prove the hypothesis in this study, we need to compare the precipitation of bacterial siderophores and Fe ions in the experiment, with iron plaque collected from *P. australis* growing at the study site via X-ray absorption fine structure analysis in the further research.

Plants accumulating high concentrations of metals should have metal-tolerance mechanisms to survive the toxicities caused by high metal concentrations [15]. In summary, *P. australis* seems to have Fe tolerance mechanisms in the epidermal cells of the nodal roots (Figure 3). Generally, metal deposition in plant cell walls inhibits metal diffusion into important cell organisms such as mitochondria and nuclei [65]. Therefore, Fe deposition in epidermal root cells contributes to tolerance in *P. australis*. Additionally, an iron plaque outside the nodal roots is vital for *P. australis* to inhibit Fe entrance into the root cells [13]. Results in this study showing the possible influence of bacterial siderophores on iron plaque formation might indirectly indicate bacterial contribution to the tolerance of *P. australis*. In future studies at the study site, we should carefully calculate the percentages of the nodal roots with an iron plaque to confirm the contribution rate of iron plaque.

In conclusion, in this study, the accumulation of Fe, Mn, and ^{238}U in the nodal roots of *P. australis* and iron plaque around the nodal roots was clarified. Lots of root-endophytic bacteria showed siderophore production activities, and the bacterial products of *Pseudomonas* spp. and *Rhizobium* spp. might influence the formation of iron plaque. Additionally, iron plaque formation around the nodal roots via the support of bacterial products by *Pseudomonas* spp. and *Rhizobium* spp., would be related to tolerance in *P. australis*; these root-endophytic bacteria might indirectly contribute to the tolerance. In the future study, we should clarify the effects of these root-endophytic bacteria via the inoculation test to *P. australis*. Although there are issues to be resolved in this research, we hope that this fundamental research on plant-microbe interactions would be helpful for phytoremediation at mine sites.

Author Contributions: Conceptualization, K.Y., K.D., T.H. and K.F.; methodology, Y.N., K.Y., T.H., K.T. and K.F.; software, Y.N.; validation, Y.N., K.Y. and K.D.; formal analysis, Y.N.; investigation, Y.N., K.Y., K.D., T.H. and K.F.; resources, K.F., K.T., N.K. and Y.O.; data curation, Y.N., K.Y., X.L. and K.D.; writing—original draft preparation, Y.N. and K.Y.; writing—review and editing, K.Y., X.L., K.D. and T.H.; Visualization, K.D. and X.L.; supervision, K.Y.; project administration, K.Y., K.F., K.T., N.K., S.F. and Y.O.; funding acquisition, K.Y. All authors have read and agreed to the published version of the manuscript.

Funding: This work was funded by Grants-in-Aid for Scientific Research (KAKENHI), grant numbers 19H01161 and 19K22151, and Ningyo-toge Environmental Engineering Center, Japan Atomic Energy Agency. This work was also supported by a Sasakawa Scientific Research Grant from the Japan Science Society.

Data Availability Statement: The data are not publicly available due to privacy.

Acknowledgments: We acknowledge the support for the field survey provided by the Ningyo-Toge Environmental Engineering Center, Japan Atomic Energy Agency.

Conflicts of Interest: The authors declare no conflict of interest. The funders had no role in the design of the study.

References

1. Dushenkov, V.; Kumar, P.B.A.N.; Motto, H.; Raskin, I. Rhizofiltration: The use of plants to remove heavy metals from aqueous streams. *Environ. Sci. Technol.* **1995**, *29*, 1239–1245. [CrossRef]
2. Janson, C.E.; Kenson, R.E.; Tucker, L.H. Treatment of heavy metals in wastewaters. What wastewater-treatment method is most cost-effective for electroplating and finishing operations? Here are the alternatives. *Environ. Prog.* **1982**, *1*, 212–216. [CrossRef]
3. Sheoran, A.S.; Sheoran, V. Heavy metal removal mechanism of acid mine drainage in wetlands: A critical review. *Miner. Eng.* **2006**, *19*, 105–116. [CrossRef]
4. Dunbabin, J.S.; Bowmer, K.H. Potential use of constructed wetlands for treatment of industrial wastewaters containing metals. *Sci. Total Environ.* **1992**, *111*, 151–168. [CrossRef]
5. Prokop, Z.; Cupr, P.; Zlevorova-Zlamalikova, V.; Komárek, J.; Dusek, L.; Holoubek, I. Mobility, bioavailability, and toxic effects of cadmium in soil samples. *Environ. Res.* **2003**, *91*, 119–126. [CrossRef]
6. Rezania, S.; Park, J.; Rupani, P.F.; Darajeh, N.; Xu, X.; Shahrokhishahraki, R. Phytoremediation potential and control of *Phragmites australis* as a green phytomass: An overview. *Environ. Sci. Pollut. Res.* **2019**, *26*, 7428–7441. [CrossRef] [PubMed]
7. Weis, J.S.; Weis, P. Metal uptake, transport and release by wetland plants: Implications for phytoremediation and restoration. *Environ. Int.* **2004**, *30*, 685–700. [CrossRef]
8. Nagayasu, T.; Taki, T.; Fukushima, S. History and current situation of mine water treatment in Ningyo-toge uranium mine. *JAEA Technol.* **2017**, *31*, 1–87. (In Japanese) [CrossRef]
9. Shitaka, Y.; Takayuki, T.; Sato, K. Evaluation of the variation of ^{226}Ra and Ca uptake by plant and their relationship. *J. Nucl. Sci. Technol.* **2002**, *39*, 958–961. [CrossRef]
10. Vymazal, J. Emergent plants used in free water surface constructed wetlands: A review. *Ecol. Eng.* **2013**, *61*, 582–592. [CrossRef]
11. Armstrong, W. Aeration in higher plants. *Adv. Bot. Res.* **1980**, *7*, 225–332. [CrossRef]
12. Ederli, L.; Reale, L.; Ferranti, F.; Pasqualini, S. Responses induced by high concentration of cadmium in *Phragmites australis* roots. *Physiol. Plant.* **2004**, *121*, 66–74. [CrossRef]
13. Peverly, J.H.; Surface, J.M.; Wang, T. Growth and trace metal absorption by *Phragmites australis* in wetlands constructed for landfill leachate treatment. *Ecol. Eng.* **1995**, *5*, 21–35. [CrossRef]
14. Wang, W.; Dudel, E.G. Fe plaque-related aquatic uranium retention via rhizofiltration along a redox-state gradient in a natural *Phragmites australis* Trin ex Steud. wetland. *Environ. Sci. Pollut. Res.* **2017**, *24*, 12185–12194. [CrossRef] [PubMed]
15. Hall, J.L. Cellular mechanisms for heavy metal detoxification and tolerance. *J. Exp. Bot.* **2002**, *53*, 1–11. [CrossRef]
16. Jiang, X.; Wang, C. Cadmium distribution and its effects on molybdate-containing hydroxylases in *Phragmites australis*. *Aquat. Bot.* **2007**, *86*, 353–360. [CrossRef]
17. Jiang, X.; Wang, C. Zinc distribution and zinc-binding forms in *Phragmites australis* under zinc pollution. *J. Plant Physiol.* **2008**, *165*, 697–704. [CrossRef] [PubMed]
18. Higuchi, K.; Tsuchiya, M.; Nakata, S.; Tanabe, A.; Fukawa, S.; Kanai, M.; Miwa, E. Detoxification of cadmium (Cd) by a novel Cd-associated and Cd-induced molecule in the stem of common reed. *J. Plant Physiol.* **2013**, *170*, 1553–1560. [CrossRef]
19. Christensen, K.K.; Sand-Jensen, K. Precipitated iron and manganese plaques restrict root uptake of phosphorus in *Lobelia dortmanna*. *Can. J. Bot.* **1998**, *76*, 2158–2163.
20. Hansel, C.M.; Fendorf, S.; Sutton, S.; Newville, M. Characterization of Fe plaque and associated metals on the roots of mine-waste impacted aquatic plants. *Environ. Sci. Technol.* **2001**, *35*, 3863–3868. [CrossRef]
21. Greipsson, S.; Crowder, A.A. Amelioration of copper and nickel toxicity by iron plaque on roots of rice (Oryza sativa). *Can. J. Bot.* **1992**, *70*, 824–830. [CrossRef]
22. Tripathi, R.D.; Tripathi, P.; Dwivedi, S.; Kumar, A.; Mishra, A.; Chauhan, P.S.; Norton, G.J.; Nautiyal, C.S. Roles for root iron plaque in sequestration and uptake of heavy metals and metalloids in aquatic and wetland plants. *Metallomics* **2014**, *6*, 1789–1800. [CrossRef]
23. Zaets, I.; Kozyrovska, N. Heavy metal resistance in plants: A putative role of endophytic bacteria. In *Toxicity of Heavy Metals to Legumes and Bioremediation*; Zaidi, A., Wani, P.A., Khan, M.S., Eds.; Springer: Vienna, Austria, 2012; pp. 203–217.
24. Varma, A. Preface. In *Microbial Siderophores*; Varma, A., Chincholkar, S., Eds.; Springer: Heidelberg, Germany, 2007; pp. V–VI.
25. Braud, A.; Jézéquel, K.; Léger, M.A.; Lebeau, T. Siderophore production by using free and immobilized cells of two pseudomonads cultivated in a medium enriched with Fe and/or toxic metals (Cr, Hg, Pb). *Biotechnol. Bioeng.* **2006**, *94*, 1080–1088. [CrossRef] [PubMed]
26. Whiting, S.N.; de Souza, M.P.; Terry, N. Rhizosphere bacteria mobilize Zn for hyperaccumulation by *Thlaspi caerulescens*. *Environ. Sci. Technol.* **2001**, *35*, 3144–3150. [CrossRef]
27. Babu, A.G.; Kim, J.D.; Oh, B.T. Enhancement of heavy metal phytoremediation by *Alnus firma* with endophytic *Bacillus thuringiensis* GDB-1. *J. Hazard. Mater.* **2013**, *250*, 477–483. [CrossRef]
28. Nagata, S.; Yamaji, K.; Nomura, N.; Ishimoto, H. Root endophytes enhance stress-tolerance of *Cicuta virosa* L. growing in a mining pond of eastern Japan. *Plant Species Biol.* **2014**, *30*, 116–125. [CrossRef]
29. Mikutta, C. X-ray absorption spectroscopy study on the effect of hydroxybenzoic acids on the formation and structure of ferrihydrite. *Geochim. Cosmochim. Acta* **2011**, *75*, 5122–5139. [CrossRef]
30. Das, A.; Prasad, R.; Srivastava, A.; Giang, P.H.; Bhatnagar, K.; Varma, A. Fungal siderophores: Structure, functions and regulation. In *Microbial Siderophores*; Varma, A., Chincholkar, S.B., Eds.; Springer: Heidelberg, Germany, 2007; pp. 8–9.

31. Bijlsma, J.; de Bruijn, W.J.C.; Hageman, J.A.; Goos, P.; Velikov, K.P.; Vincken, J.P. Revealing the main factors and two-way interactions contributing to food discolouration caused by iron-catechol complexation. *Sci. Rep.* **2020**, *10*, 8288. [CrossRef]
32. Ejima, H.; Richardson, J.J.; Caruso, F. Metal-phenolic networks as a versatile platform to engineer nanomaterials and bio-interfaces. *Nano Today* **2017**, *12*, 136–148. [CrossRef]
33. Ministry of Education, Culture, Sports, Science and Technology. *No.14 Uranium Analysis*, 2nd ed.; Japan Chemical Analysis Center: Chiba, Japan, 2002. (In Japanese)
34. Mendez, M.O.; Maier, R.M. Phytostabilization of mine tailings in arid and semiarid environments—An emerging remediation technology. *Environ. Health Perspect.* **2008**, *116*, 278–283. [CrossRef]
35. Ghosh, M.; Singh, S.P. A comparative study of cadmium phytoextraction by accumulator and weed species. *Environ. Pollut.* **2005**, *133*, 365–371. [CrossRef] [PubMed]
36. Stacey, M.G.; Patel, A.; McClain, W.E.; Mathieu, M.; Remley, M.; Rogers, E.E.; Gassmann, W.; Blevins, D.G.; Stacey, G. The *Arabidopsis* AtOPT3 protein functions in metal homeostasis and movement of iron to developing seeds. *Plant Physiol.* **2008**, *146*, 589–601. [CrossRef]
37. Giovannetti, M.; Mosse, B. An evaluation of techniques for measuring vesicular *arbuscular mycorrhizal* infection in roots. *New Phytol.* **1980**, *84*, 489–500. [CrossRef]
38. McGonigle, T.P.; Miller, M.H.; Evans, D.G.; Fairchild, G.L.; Swan, J.A. A new method which gives an objective measure of colonization of roots by vesicular—Arbuscular mycorrhizal fungi. *New Phytol.* **1990**, *115*, 495–501. [CrossRef]
39. Alexander, D.B.; Zuberer, D.A. Use of chrome azurol S reagents to evaluate siderophore production by rhizosphere bacteria. *Biol. Fertil. Soils* **1991**, *12*, 39–45. [CrossRef]
40. Lane, D.J. 16S/23S rRNA sequencing. In *Nucleic Acid Techniques in Bacterial Systematics*; Stackebrandt, E., Goodfellow, M., Eds.; John Wiley and Sons: New York, NY, USA, 1991; pp. 115–175.
41. Fukuda, A.; Hagiwara, H.; Ishimura, T.; Kouduka, M.; Ioka, S.; Amano, Y.; Tsunogai, U.; Suzuki, Y.; Mizuno, T. Geomicrobiological properties of ultra-deep granitic groundwater from the Mizunami underground research laboratory (MIU), central Japan. *Microb. Ecol.* **2010**, *60*, 214–225. [CrossRef] [PubMed]
42. Muyzer, G.; de Waal, E.C.; Uitterlinden, A.G. Profiling of complex microbial populations by denaturing gradient gel electrophoresis analysis of polymerase chain reaction-amplified genes coding for 16S rRNA. *Appl. Environ. Microb.* **1993**, *59*, 695–700. [CrossRef] [PubMed]
43. Buyer, J.S.; Sikora, L.J.; Chaney, R.L. A new growth medium for the study of siderophore-mediated interactions. *Biol. Fertil. Soils* **1989**, *8*, 97–101. [CrossRef]
44. Yamaji, K.; Ichihara, Y. The role of catechin and epicatechin in chemical defense against damping-off fungi of current-year *Fagus crenata* seedlings in natural forest. *For. Pathol.* **2012**, *42*, 1–7. [CrossRef]
45. Kabata-Pendias, A. *Trace Elements in Soils and Plants*, 4th ed.; CRC Press: Boca Raton, FL, USA, 2011; pp. 201–223.
46. Ali, N.A.; Bernal, M.P.; Ater, M. Tolerance and bioaccumulation of cadmium by *Phragmites australis* grown in the presence of elevated concentrations of cadmium, copper, and zinc. *Aquat. Bot.* **2004**, *80*, 163–176. [CrossRef]
47. Favas, P.J.C.; Pratas, J.; Mitra, S.; Sarkar, S.K.; Venkatachalam, P. Biogeochemistry of uranium in the soil-plant and water-plant systems in an old uranium mine. *Sci. Total. Environ.* **2016**, *568*, 350–368. [CrossRef]
48. Otte, M.L.; Rozema, J.; Koster, L.; Haarsma, M.S.; Broekman, R.A. Iron plaque on roots of *Aster tripolium* L.: Interaction with zinc uptake. *New Phytol.* **1989**, *111*, 309–317. [CrossRef]
49. Park, T.; Kim, W.I.; Kim, B.J.; Lee, H.; Choi, I.S.; Park, J.H.; Cho, W.K. Salt-induced, continuous deposition of supramolecular iron (III)–tannic acid complex. *Langmuir* **2018**, *34*, 12318–12323. [CrossRef] [PubMed]
50. Shin, M.; Park, E.; Lee, H. Plant-inspired pyrogallol-containing functional materials. *Adv. Funct. Mater.* **2019**, *29*, 1903022. [CrossRef]
51. Saha, R.; Saha, N.; Donofrio, R.S.; Bestervelt, L.L. Microbial siderophores: A mini review. *J. Basic Microbiol.* **2013**, *53*, 303–317. [CrossRef] [PubMed]
52. Budzikiewicz, H. Siderophores of fluorescent pseudomonads. *Z. Naturforsch. C* **1997**, *52*, 713–720. [CrossRef]
53. Teintze, M.; Hossain, M.B.; Barnes, C.L.; Leong, J.; Van der Helm, D. Structure of ferric pseudobactin: A siderophore from a plant growth promoting *Pseudomonas*. *Biochemistry* **1981**, *20*, 6446–6457. [CrossRef] [PubMed]
54. Cox, C.D.; Rinehart, K.L., Jr.; Moore, M.L.; Cook, J.C., Jr. Pyochelin: Novel structure of an iron-chelating growth promoter for *Pseudomonas aeruginosa*. *Proc. Natl. Acad. Sci. USA* **1981**, *78*, 4256–4260. [CrossRef]
55. Mossialos, D.; Meyer, J.-M.; Budzikiewicz, H.; Wolff, U.; Koedam, N.; Baysse, C.; Anjaiah, V.; Cornelis, P. Quinolobactin, a new siderophore of *Pseudomonas fluorescens* ATCC 17400, the production of which is repressed by the cognate pyoverdine. *Appl. Environ. Microbiol.* **2000**, *66*, 487–492. [CrossRef]
56. Risse, D.; Beiderbeck, H.; Taraz, K.; Budzikiewicz, H.; Gustine, D. Corrugatin, a lipopeptide siderophore from *Pseudomonas corrugata*. *Z. Naturforsch. C* **1998**, *53*, 295–304. [CrossRef]
57. Matthijs, S.; Budzikiewicz, H.; Schäfer, M.; Wathelet, B.; Cornelis, P. Ornicorrugatin, a new siderophore from *Pseudomonas fluorescens* AF76. *Z. Naturforsch. C* **2008**, *63*, 8–12. [CrossRef]
58. Anthoni, U.; Christophersen, C.; Nielsen, P.H.; Gram, L.; Petersen, B.O. Pseudomonine, an isoxazolidone with siderophoric activity from *Pseudomonas fluorescens* AH2 isolated from Lake Victorian Nile perch. *J. Nat. Prod.* **1995**, *58*, 1786–1789. [CrossRef]

59. Rosconi, F.; Davyt, D.; Martínez, V.; Martínez, M.; Abin-Carriquiry, J.A.; Zane, H.; Butler, A.; de Souza, E.M.; Fabiano, E. Identification and structural characterization of serobactins, a suite of lipopeptide siderophores produced by the grass endophyte *Herbaspirillum seropedicae*. *Environ. Microbiol.* **2013**, *15*, 916–927. [CrossRef]
60. Smith, M.J.; Shoolery, J.N.; Schwyn, B.; Holden, I.; Neilands, J.B. Rhizobactin, a structurally novel siderophore from Rhizobium meliloti. *J. Am. Chem. Soc.* **1985**, *107*, 1739–1743. [CrossRef]
61. Dilworth, M.J.; Carson, K.C.; Giles, R.G.F.; Byrne, L.T.; Glenn, A.R. *Rhizobium leguminosarum* bv. viciae produces a novel cyclic trihydroxamate siderophore, vicibactin. *Microbiology* **1998**, *144*, 781–791. [CrossRef] [PubMed]
62. Storey, E.P.; Boghozian, R.; Little, J.L.; Lowman, D.W.; Chakraborty, R. Characterization of 'Schizokinen'; a dihydroxamate-type siderophore produced by Rhizobium leguminosarum IARI 917. *Biometals* **2006**, *19*, 637–649. [CrossRef]
63. Patel, H.N.; Chakraborty, R.N.; Desai, S.B. Isolation and partial characterization of phenolate siderophore from *Rhizobium leguminosarum* IARI 102. *FEMS Microbiol. Lett.* **1988**, *56*, 131–134. [CrossRef]
64. Modi, M.; Shah, K.S.; Modi, V.V. Isolation and characterization of catechol-like siderophore from cowpea *Rhizobium* RA-1. *Arch. Microbiol.* **1985**, *141*, 156–158. [CrossRef]
65. Krzesłowska, M. The cell wall in plant cell response to trace metals: Polysaccharide remodeling and its role in defense strategy. *Acta Physiol. Plant.* **2011**, *33*, 35–51. [CrossRef]